Disruption of the ATXN1-CIC complex causes a spectrum of neurobehavioral phenotypes in mice and humans

Hsiang-Chih Lu, Qiumin Tan, Maxime WC Rousseaux, Wei Wang, Ji-Yoen Kim, Ronald Richman, Ying-Wooi Wan, Szu-Ying Yeh, Jay M Patel, Xiuyun Liu, Tao Lin, Yoontae Lee, John D Fryer, Jing Han, Maria Chahrour, Richard H Finnell, Yunping Lei, Maria E Zurita-Jimenez, Priyanka Ahimaz, Kwame Anyane-Yeboa, Lionel Van Maldergem, Daphne Lehalle, Nolwenn Jean-Marcais, Anne-Laure Mosca-Boidron, Julien Thevenon, Margot A Cousin, Della E Bro, Brendan C Lanpher, Eric W Klee, Nora Alexander, Matthew N Bainbridge, Harry T Orr, Roy V Sillitoe, M. Cecilia Ljungberg, Zhandong Liu, Christian P Schaaf, Huda Y Zoghbi

Supplementary Figures

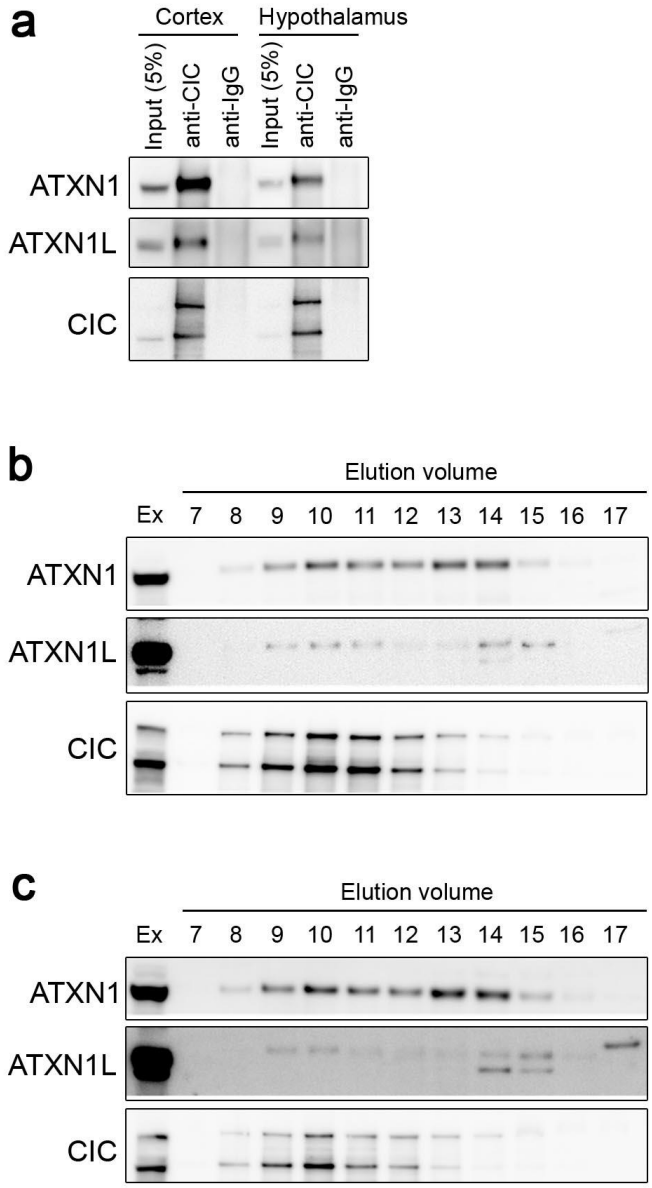

Supplementary Figure 1. ATXN1-CIC complex is found in the cortex and hypothalamus. (**a**) Co-immunoprecipitation of ATXN1 and ATXN1L with CIC from wild-type mouse cortex and hypothalamus extracts. **(b, c)** Western blots of gel-filtration fractions of wildtype mouse (**b**) cortex and (**c**) hypothalamus extracts were analyzed for ATXN1, ATXN1L, and CIC. The ATXN1-CIC complex co-eluted in fractions 9-11. Ex, tissue total protein extract.

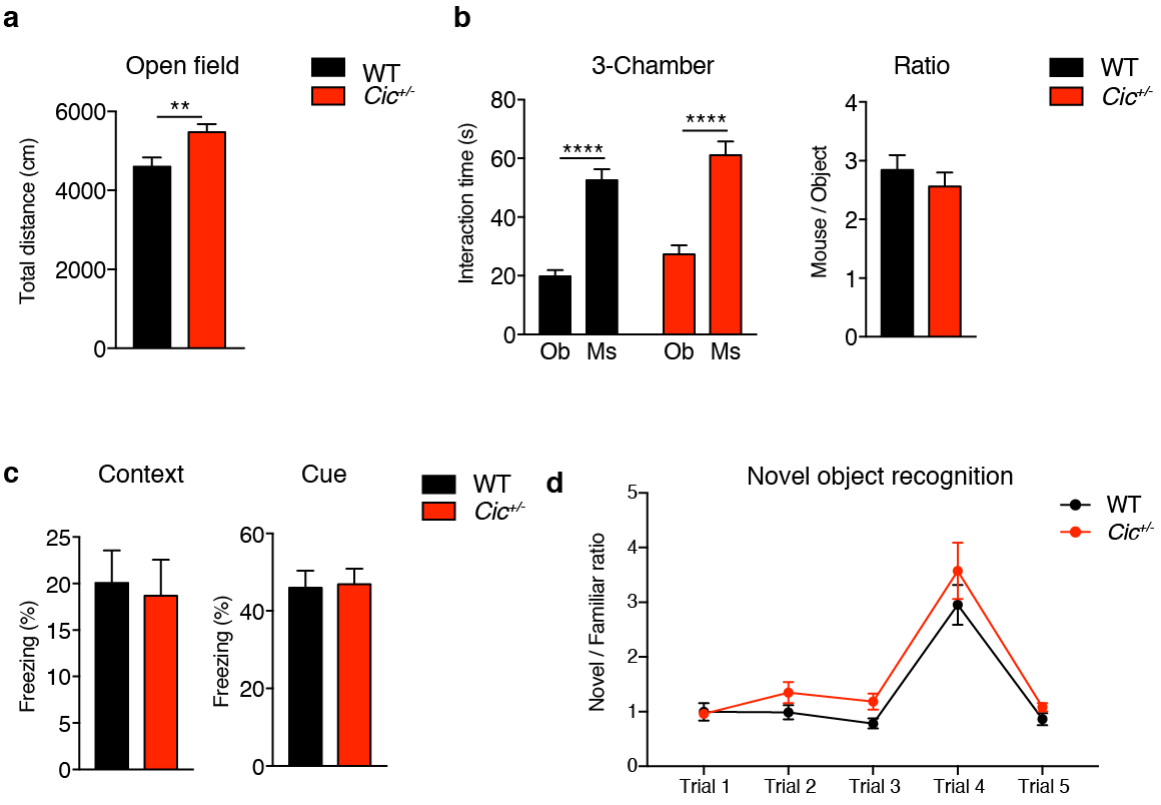

Supplementary Figure 2. *Cic*$^{+/-}$ mice are slightly hyperactive. (**a**) The *Cic*$^{+/-}$ mice showed a mild increase in exploratory activity in the open field test compared to wildtype littermates (n = 29-38). (**b**) *Cic*$^{+/-}$ mice had normal social interaction in the three-chamber test (n = 11-18). Ob, object; Ms, mouse. (**c, d**) *Cic*$^{+/-}$ mice displayed normal learning and memory in the fear-conditioning assay and novel object recognition test (n = 14-19). Data are represented as mean ± s.e.m. **: $P < 0.05$; ****: $P < 0.0001$

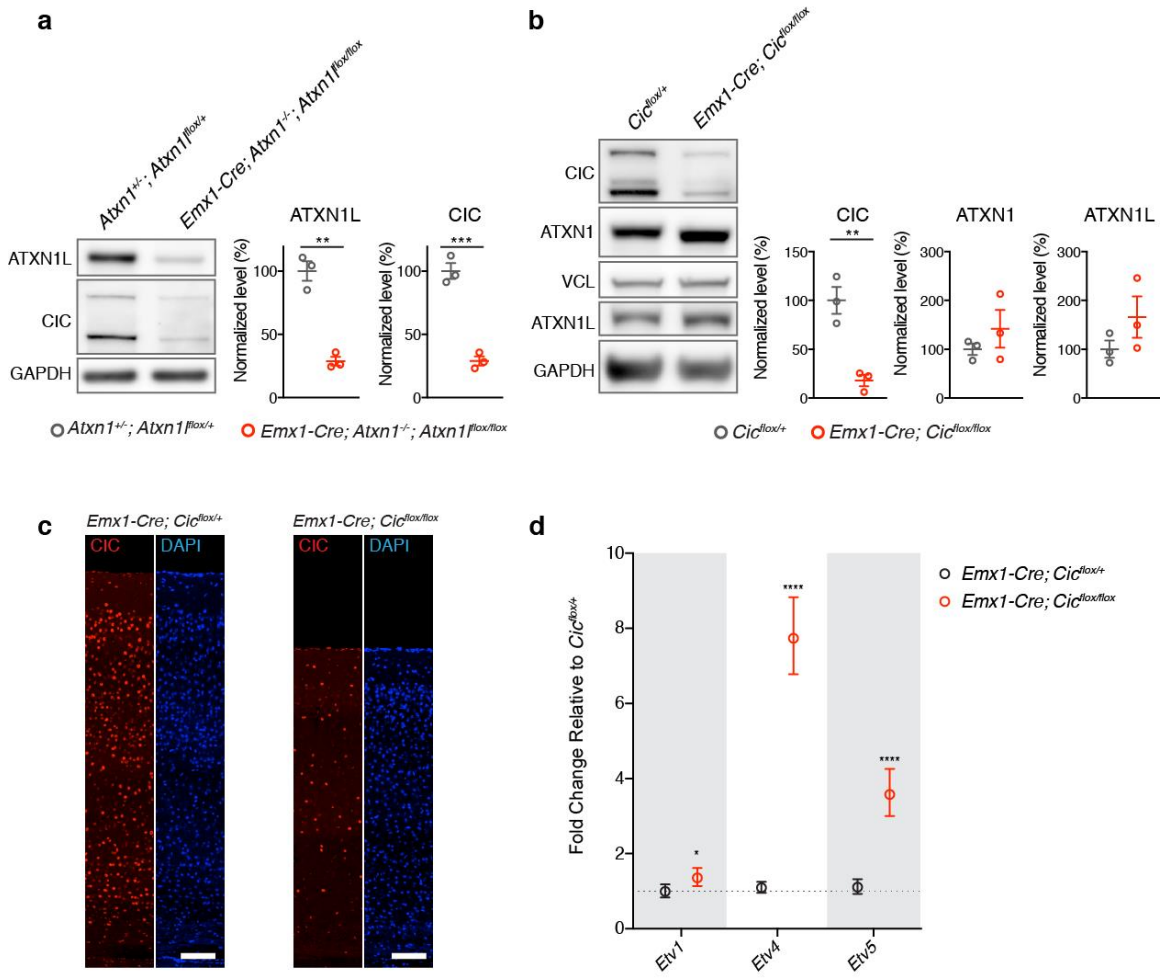

Supplementary Figure 3. *Emx1*-Cre removes the floxed allele efficiently; known CIC target genes are upregulated in *Cic* conditional knockouts. (**a**) ATXN1L protein levels were significantly reduced in the conditional knockout mouse brain tissue. CIC protein levels were also reduced in *Atxn1-Atxn1l* mutant (n = 3). (**b**) Western blot from mutant and control mice showed that CIC was efficiently removed, but the protein levels of ATXN1 and ATXN1L remained largely unaffected (n = 3). (**c**) Immunofluorescent staining of cortex from control and mutant animals with CIC antibody showing that knockout efficiency was consistent across different cortical layers. The remaining CIC immunoreactivity came from inhibitory neurons and

non-neuroglial cell types (Scale bar = 100 μm). (**d**) *Etv1/4/5*, which are known genes repressed by CIC, were upregulated in the cortex of E18.5 *Cic* conditional knockout animals (n = 3). Data are represented as mean ± s.e.m. (**a, b**) or c.i. (**d**). *: $P < 0.05$; **: $P < 0.01$; ***: $P < 0.001$; ****: $P < 0.0001$

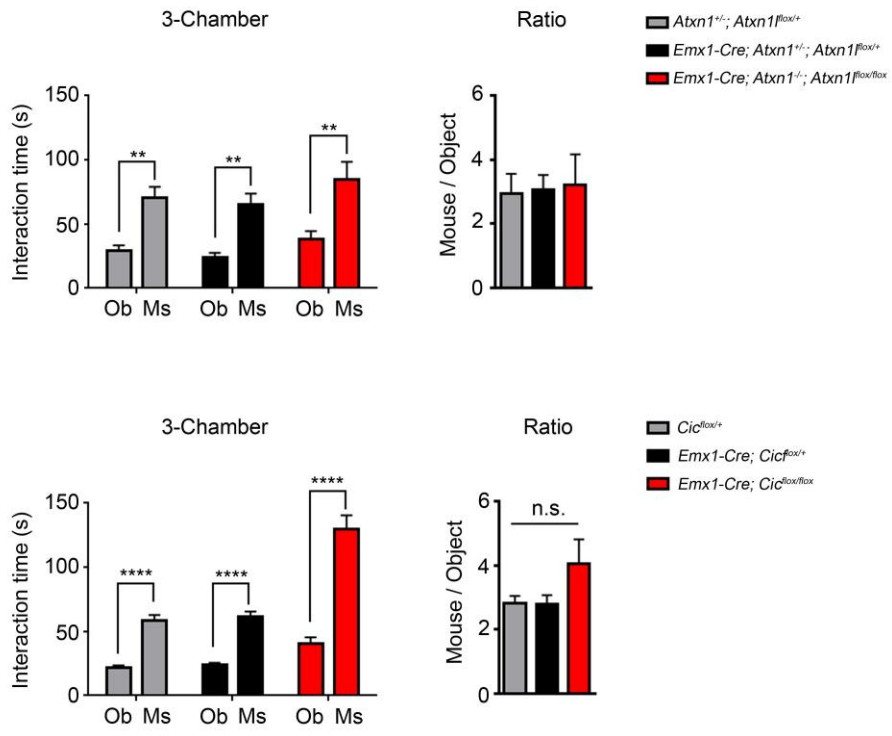

Supplementary Figure 4. *Emx1-Cre Atxn1-Atxn1l* and *Cic* conditional mutants show normal social interaction in the three-chamber test. Upper panels, *Emx1-Cre Atxn1-Atxn1l* mutants, n = 8-13; lower panels, *Emx1-Cre Cic* mutants, n = 14-15. Ob, object; Ms, mouse. Data are represented as mean ± s.e.m. **: $P < 0.01$; ****: $P < 0.0001$. n.s.: not significant.

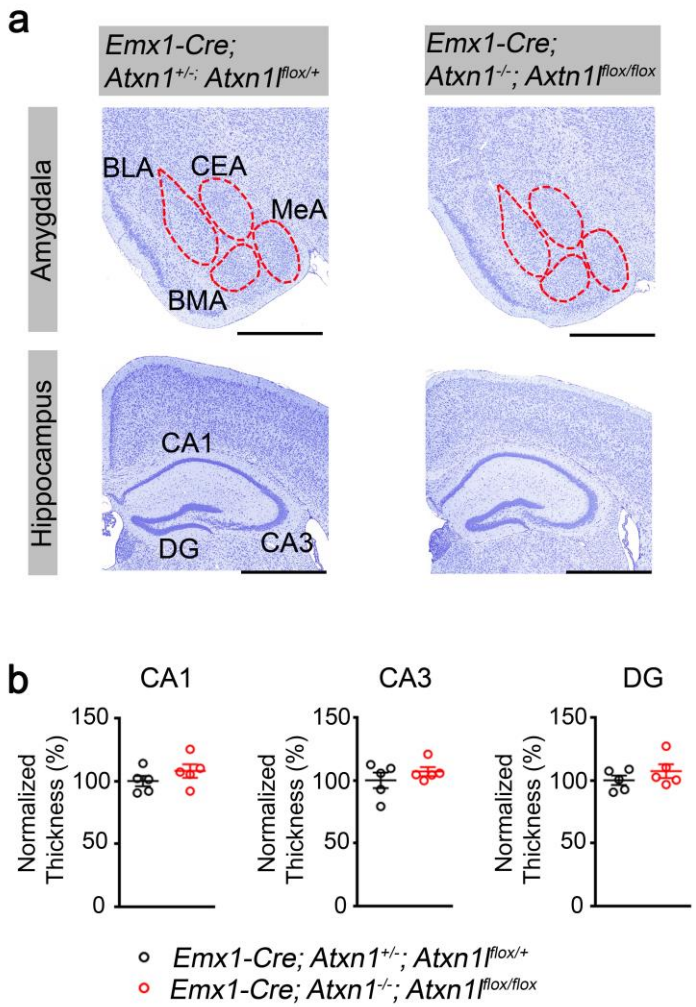

Supplementary Figure 5. Normal structures of amygdala and hippocampus in five-week old *Emx1-Cre Atxn1-Atxn1l* mice.

(**a**) Nissl staining of five-week old brain sections showing normal structure and cellularity of amygdala and hippocampus in mutant mice (scale bar = 1 mm). BLA, basolateral amygdala; CEA, central nucleus of the amygdala; BMA, basomedial amygdala; MeA, medial amygdala; DG, dentate gyrus. (**b**) Quantification of the thickness of pyramidal layers of CA1 and CA3, and the granule layer thickness of DG (n = 5). Data are represented as mean ± s.e.m.

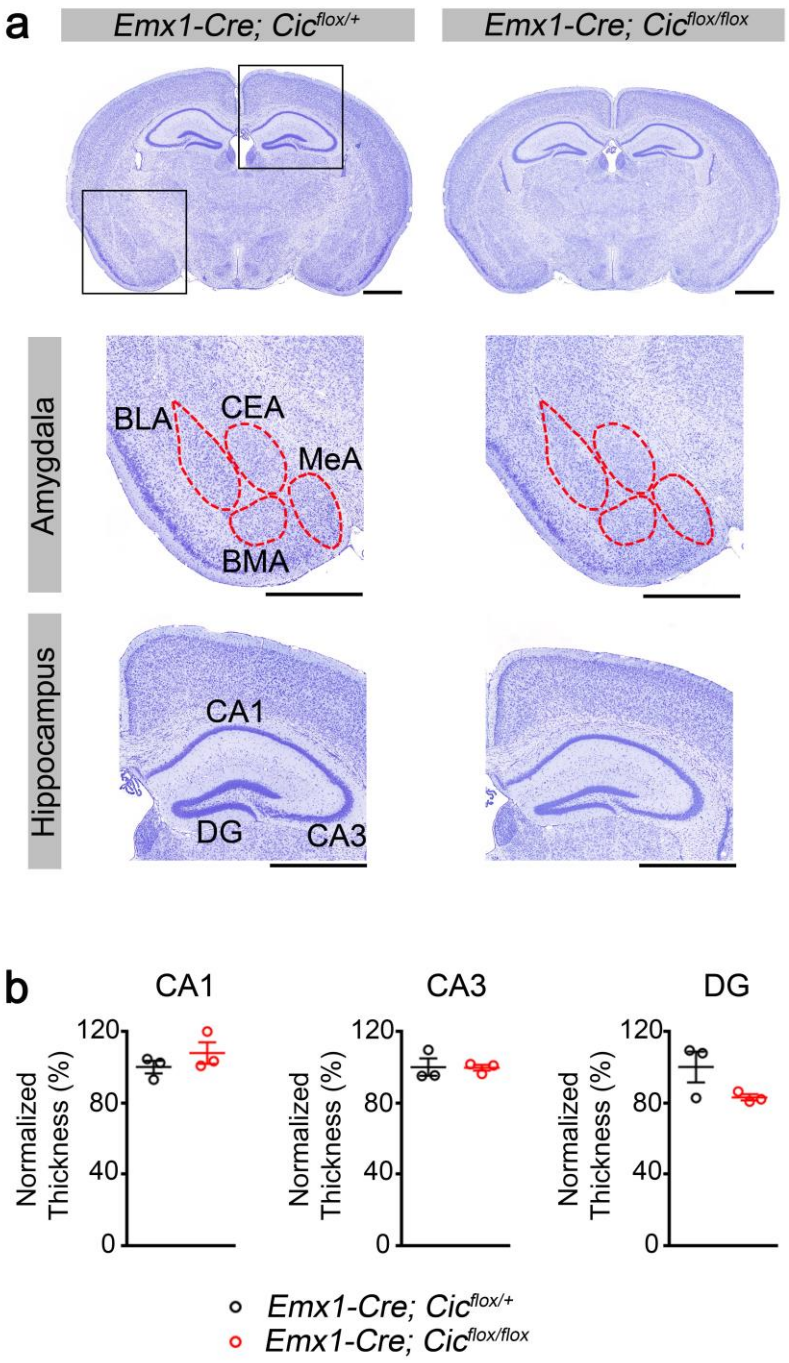

Supplementary Figure 6. Normal structures of amygdala and hippocampus in five-week old *Emx1-Cre Cic* mice.

(**a**) Nissl staining of five-week old brain sections showing normal structure and cellularity of amygdala and hippocampus in mutant mice (scale bar = 1 mm). BLA, basolateral amygdala;

CEA, central nucleus of the amygdala; BMA, basomedial amygdala; MeA, medial amygdala; DG, dentate gyrus. (**b**) Quantification of the thickness of pyramidal layers of CA1 and CA3, and the granule layer thickness of DG (n = 3). Data are represented as mean ± s.e.m.

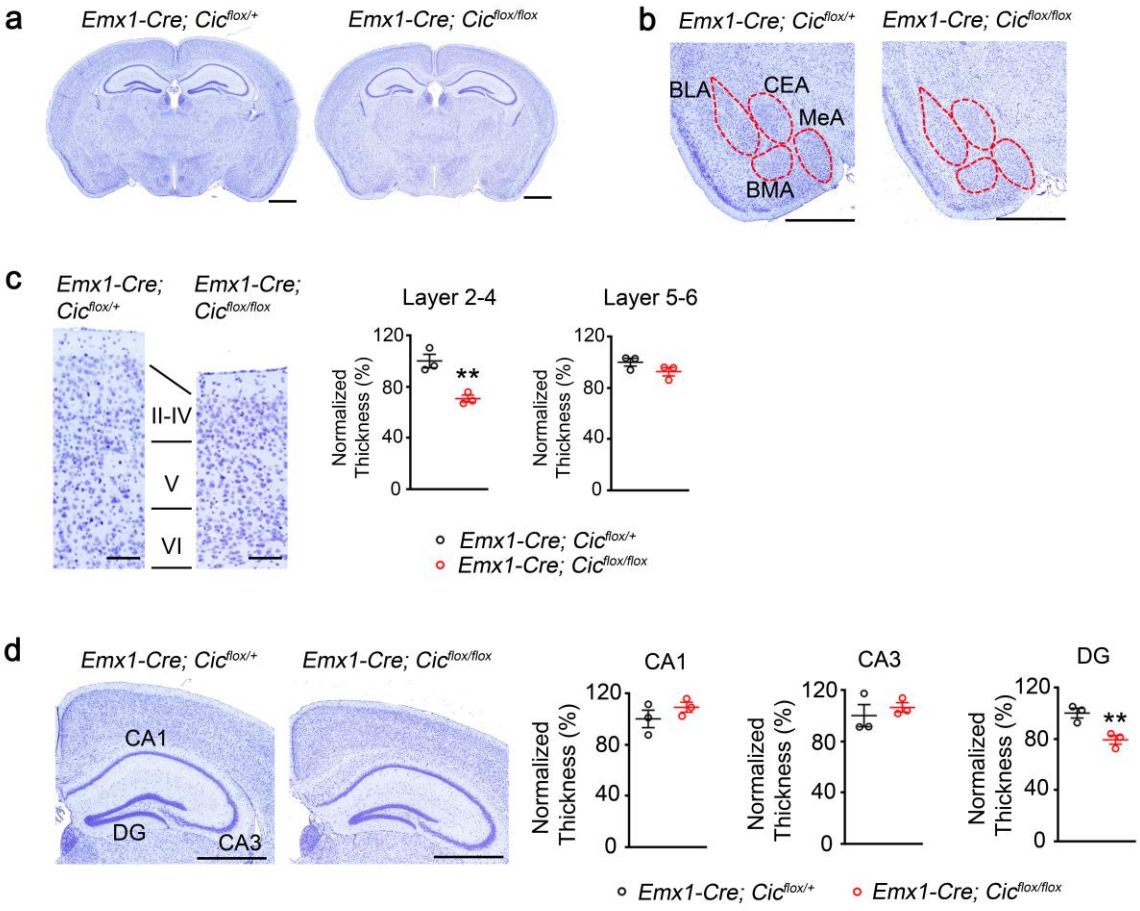

Supplementary Figure 7. Anatomical defects in 20-week old *Emx1-Cre Cic* conditional knockout brain revealed by Nissl staining.

(**a**) Whole brain coronal sections of control (*Emx1-Cre; Cic*$^{flox/+}$) and mutant mice (*Emx1-Cre; Cic*$^{flox/flox}$) (Scale bar = 1 mm). (**b**) The structures of multiple amygdala nucleus were comparable between control and mutant animals (scale bar = 1 mm). BLA, basolateral amygdala; CEA, central nucleus of the amygdala; BMA, basomedial amygdala; MeA, medial amygdala. (**c**) The thickness of layer 2-4 was reduced in mutant mice, while that of layer 5-6 remained similar to controls (scale bar = 200 μm; n = 3). (**d**) The thickness of dentate gyrus granule layer was decreased in mutant hippocampus, whereas CA1 and CA3 remained normal. DG, dentate gyrus. (scale bar = 200 μm; n = 3). Data are represented as mean ± s.e.m. **: $P < 0.01$

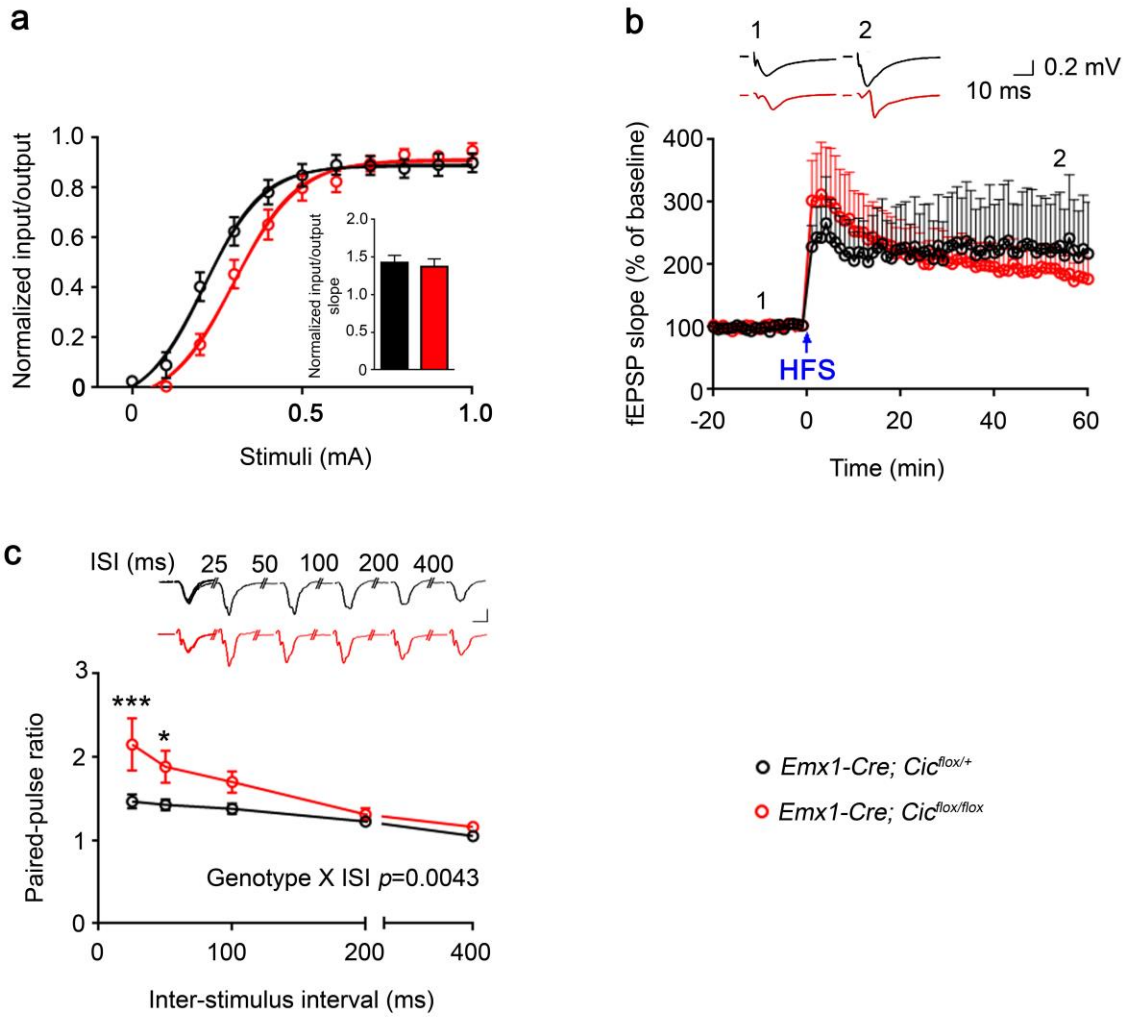

Supplementary Figure 8. Analyses of hippocampal synaptic transmission and plasticity in *Emx1-Cre Cic* mutant mice.

(**a**) There was no significant difference in the slopes of input-output (I/O) curves from hippocampal Schaffer collateral-CA1 synapses between *Emx1-Cre; Cic*$^{flox/+}$ and *Emx1-Cre; Cic*$^{flox/flox}$ mice. The bar graph inset shows the mean slope of input-output curves. (**b**) High frequency stimulation (HFS) protocol induced similar LTP between *Emx1-Cre; Cic*$^{flox/+}$ and *Emx1-Cre; Cic*$^{flox/flox}$ mice. Superimposed representative recordings were shown for fEPSPs recorded 20 min before and 55 min after HFS. (**c**) There was an increase in the paired-pulse ratio

at 25 and 50 ms inter-pulse intervals in the *Emx1-Cre; Cic*$^{flox/flox}$ mice. These results suggest that loss of *Cic* induced a decrease in the probability of presynaptic neurotransmitter release. Top, superimposed paired-pulse fEPSPs at 25-400 ms inter-pulse intervals. Scale X=10 ms; Y=0.2 mV. (n = 3-4 animals, 2-5 slices/animal). *: $P < 0.05$; ***: $P < 0.001$

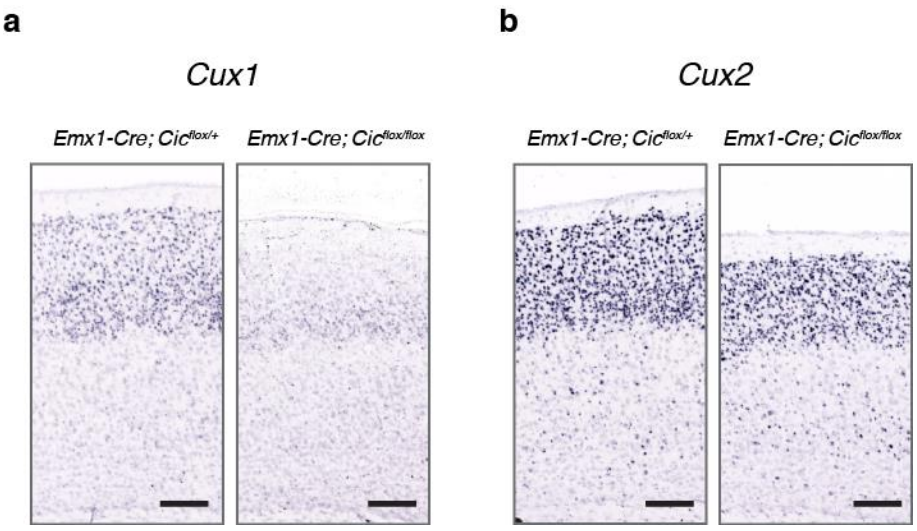

Supplementary Figure 9. *In situ* hybridization of *Cux1* and *Cux2* in the parietal cortex.

(**a**) Similar to the protein levels, the RNA expression levels of *Cux1* were reduced in the mutant cortex, whereas (**b**) the expression levels of *Cux2* remained unchanged (scale bar = 200 μm).

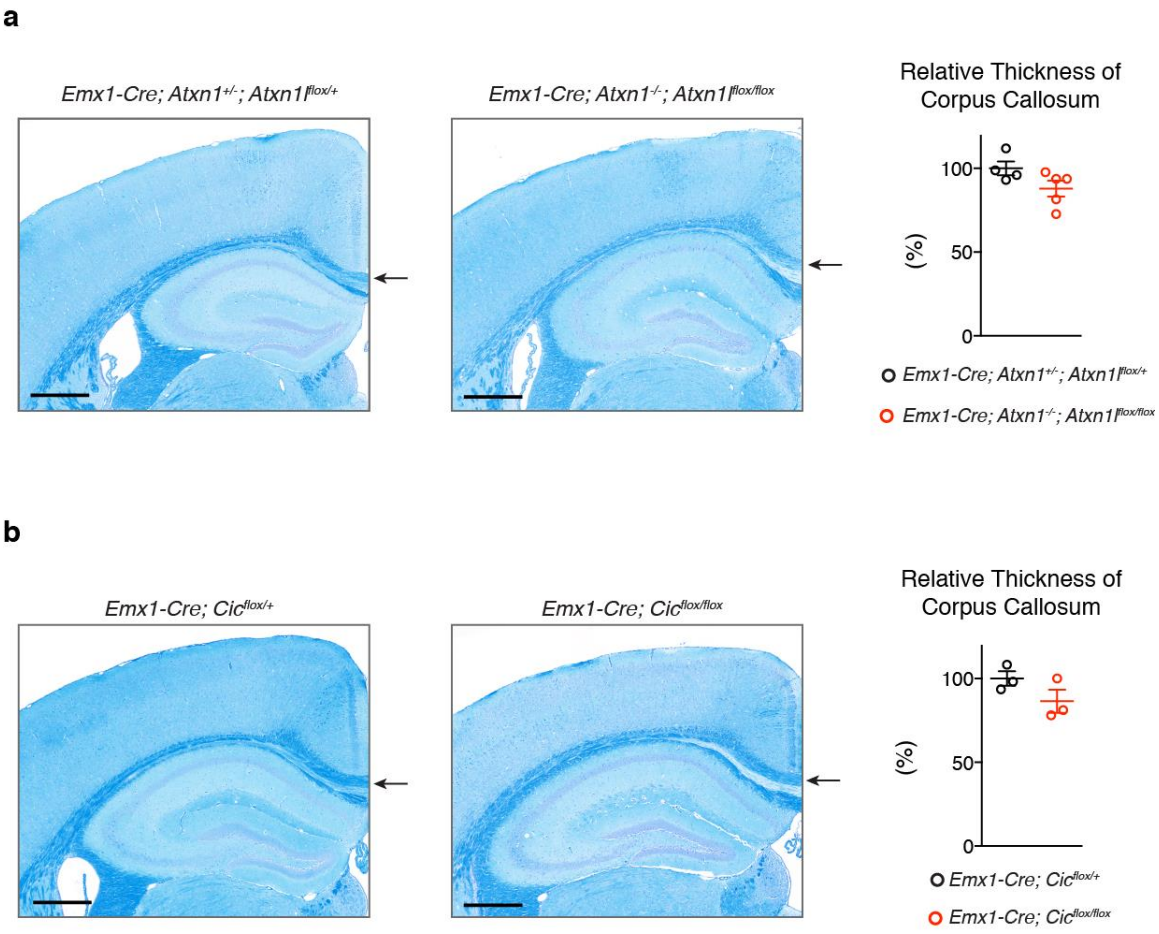

Supplementary Figure 10. The formation of corpus callosum is not disrupted in the *Emx1-Cre Atxn1-Atxn1l* or *Cic* conditional knockout mice.

Luxol Fast Blue staining of the cortex showed that the formation and the thickness of corpus callosum were not significantly altered in *Atxn1-Atxn1l* (**a**) or *Cic* (**b**) conditional knockouts. The sections were counterstained with cresyl violet (scale bar = 500 μm). Data are represented as mean ± s.e.m.

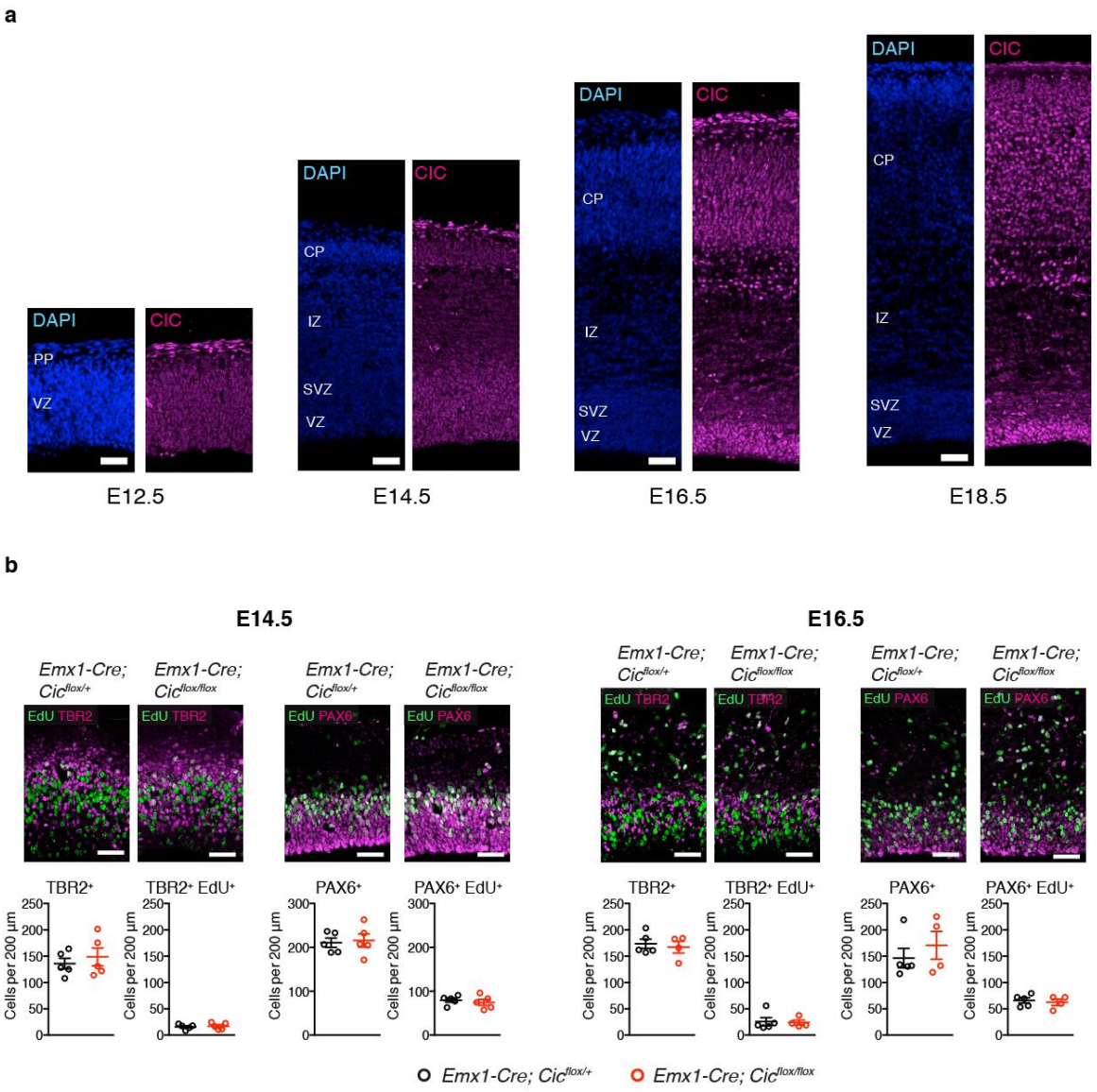

Supplementary Figure 11. *Emx1-Cre Cic* mutants exhibit normal progenitor proliferation. (**a**) Immunofluorescent staining shows that CIC was expressed in the ventricular zone (VZ and pre-plate (PP) at E12.5. Starting at E14.5, CIC expression can also be observed in subventricular zone (SVZ) and cortical plate (CP). CIC expression was lower in intermediate zone (IZ) (scale bar = 50 µm). (**b**) The proliferation of progenitors was evaluated with 2-hour pulse labeling of EdU at E14.5 and E16.5. EdU incorporated during S-phase was labeled with Alexa Fluor, and the sections were co-stained with markers for intermediate progenitors (TBR2) or radial glia

(PAX6). The numbers of $TBR2^+$ intermediate progenitors and $PAX6^+$ radial glia did not change in the mutants, nor did the number of progenitors that were double-positive for EdU, which suggests that the proliferation rate of the progenitors was unaffected (n = 5, scale bar = 50 μm). Data are represented as mean ± s.e.m.

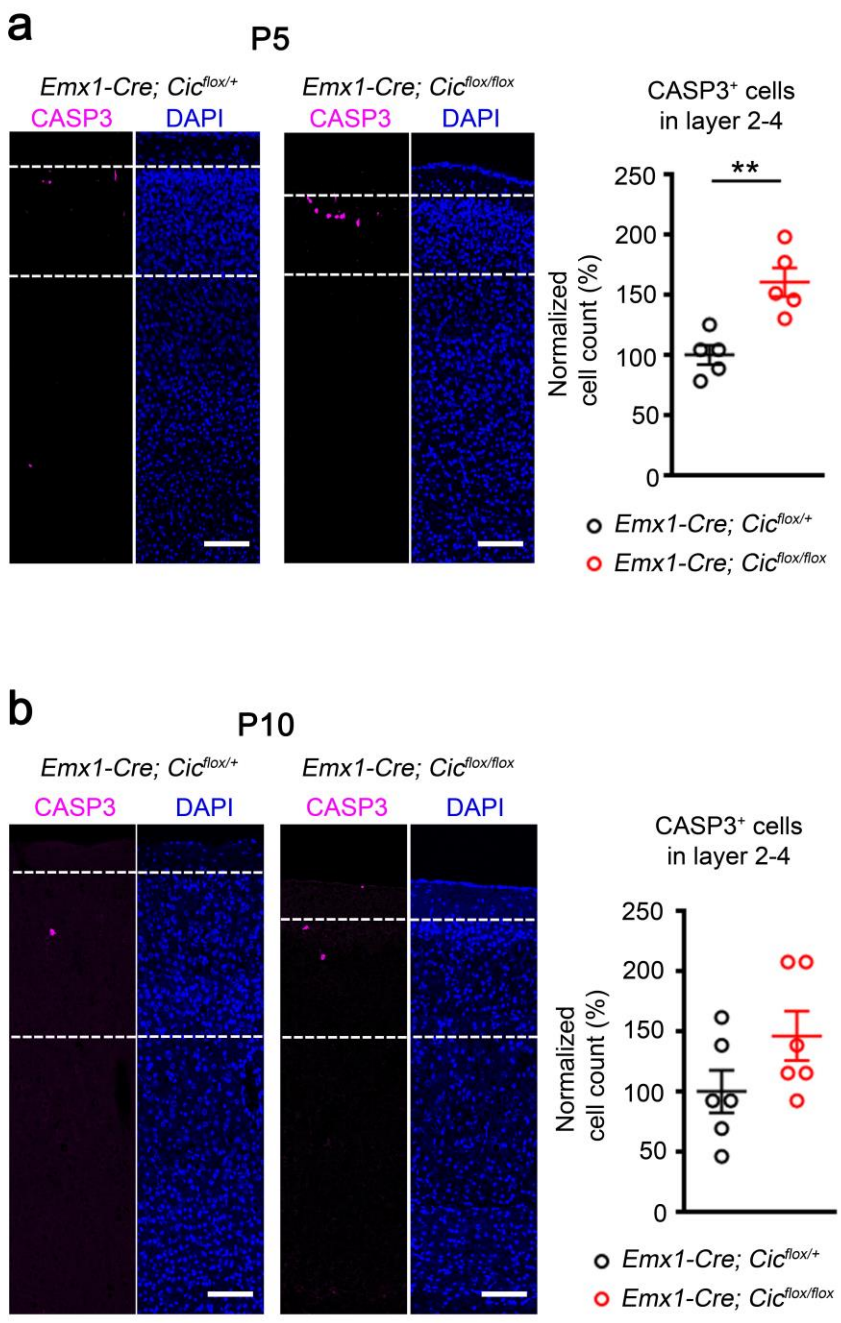

Supplementary Figure 12. A higher number of layer 2-4 cells in *Emx1-Cre Cic* mutant undergo apoptosis at P5.

Immunofluorescent staining of cortex from control and mutant animals with activated caspase-3 (CASP3) antibody showing that the number of $CASP3^{+}$ cells in layer 2-4 were increased in the

mutant cortex at P5 (**a**) but not P10 (**b**). (n = 5-6; scale bar = 200 μm). Data are represented as mean ± s.e.m. **: $P < 0.01$

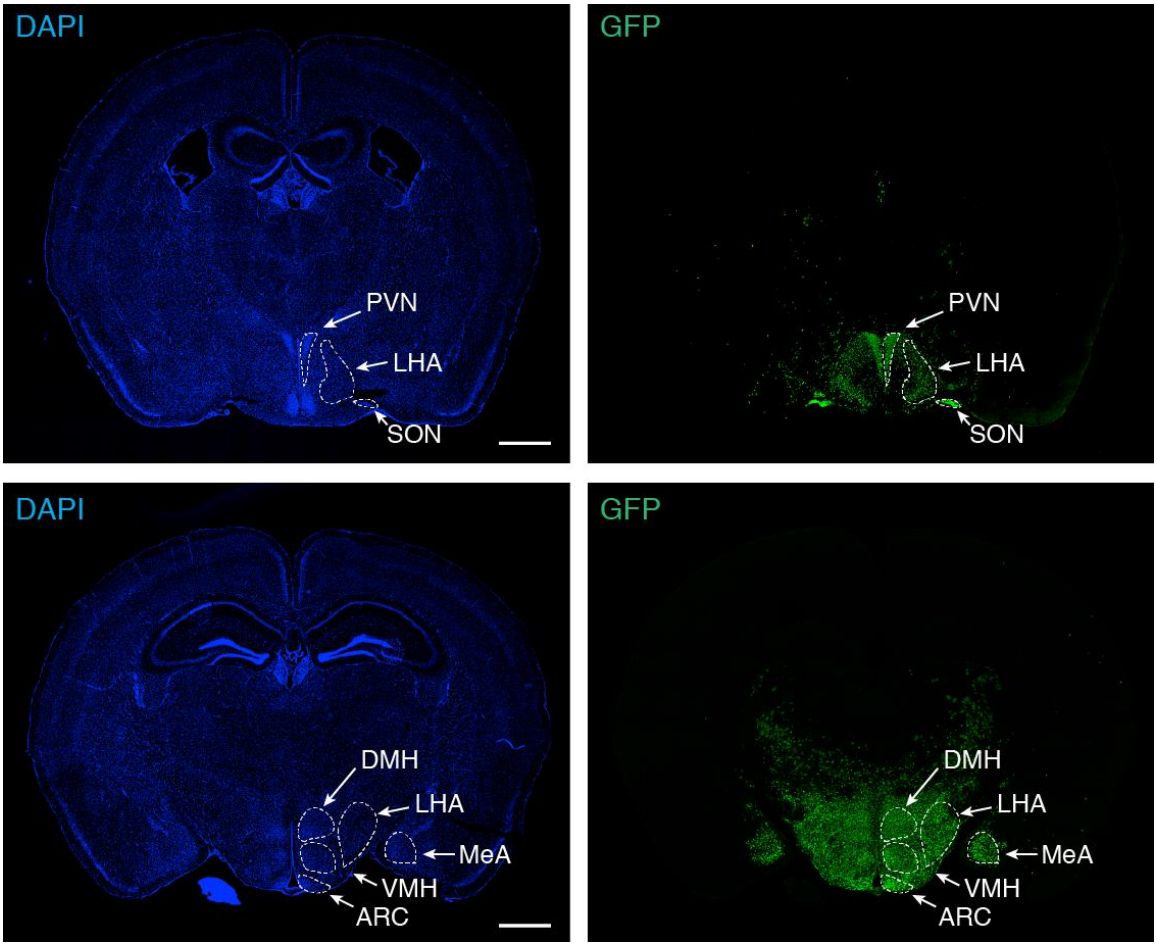

Supplementary Figure 13. Expression pattern of *Otp-Cre*.

The expression pattern of *Otp-Cre* was visualized by GFP staining with the *ROSA*^{fsTRAP}. Cre is highly expressed in paraventricular nucleus (PVN), supraoptic nucleus (SON), ventromedial hypothalamus (VMH), dorsomedial hypothalamus (DMH), lateral hypothalamic area (LHA), arcuate nucleus (ARC), and medial amygdala (MeA) (Scale bar = 1 mm).

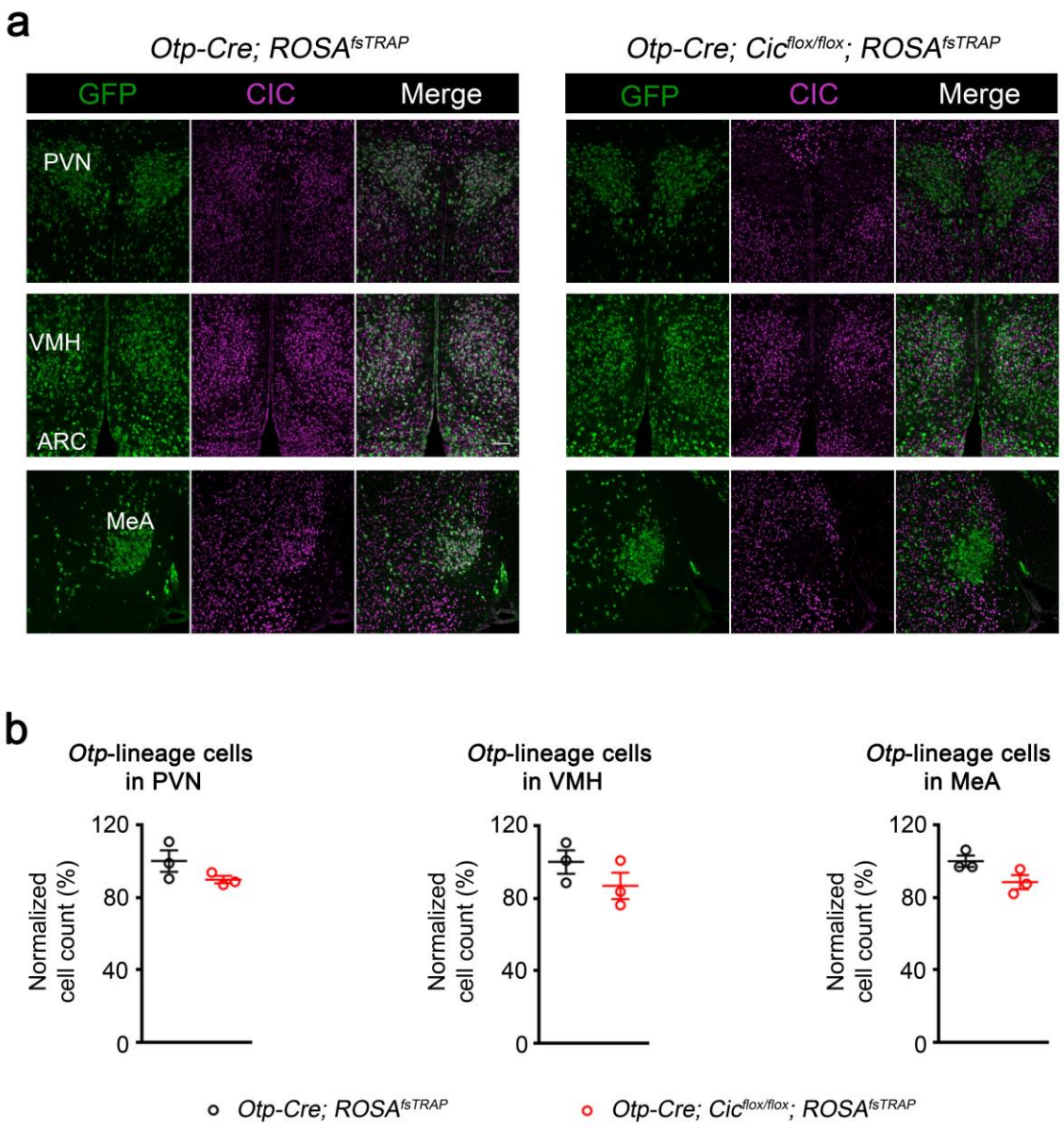

Supplementary Figure 14. *Otp-Cre* removes *Cic* efficiently without causing overt morphological defects.

(**a**) Immunofluorescent staining with CIC in the paraventricular nucleus (PVN), ventromedial hypothalamus (VMH), arcuate nucleus (ARC), and medial amygdala (MeA). CIC staining was undetectable in most cells expressing Cre (marked by GFP staining) (scale bar = 200 μm). (**b**) The numbers of *Otp*-lineage cells (marked by GFP staining) in the PVN, VMH, and MeA were

quantified in *Otp-Cre; ROSA*^{fsTRAP} and *Otp-Cre; Cic*$^{flox/flox}$*; ROSA*^{fsTRAP} mice (n = 3). Data are represented as mean ± s.e.m.

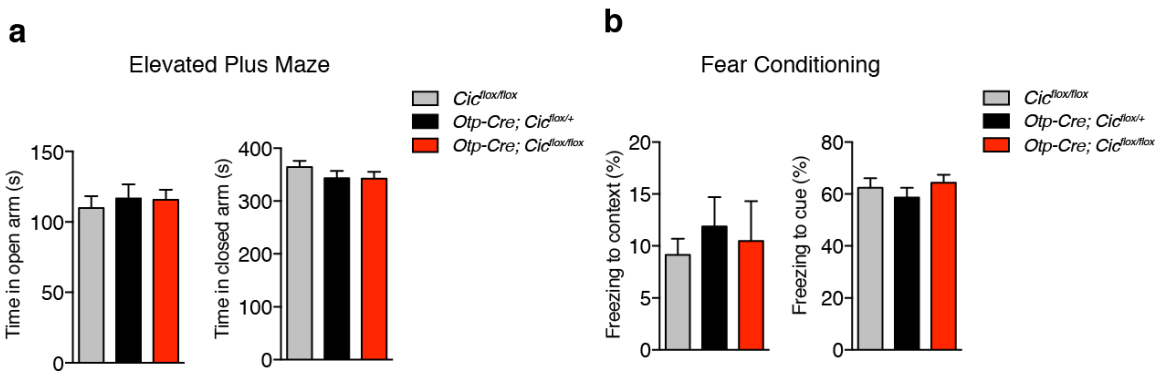

Supplementary Figure 15. *Otp-Cre Cic* conditional mutants do not show behavioral defects in the elevated plus maze or the fear conditioning test.

(**a**) *Otp-Cre Cic* mice displayed normal impulsivity/anxiety in the elevated plus maze test compared to the controls (n = 14-27). (**b**) *Otp-Cre Cic* mice had normal learning and memory compared to the controls in the fear conditioning test (n = 16-18). Data are represented as mean ± s.e.m.

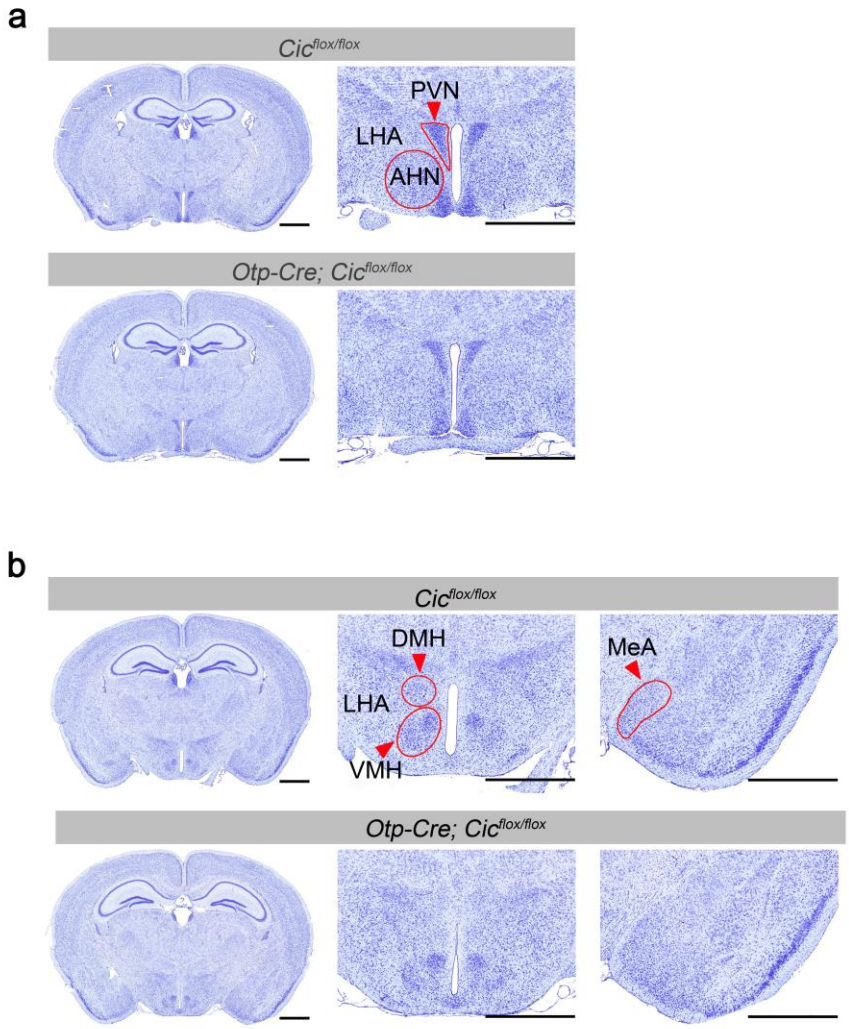

Supplementary Figure 16. *Otp-Cre Cic* mutants have normal structures of hypothalamus and medial amygdala.

Nissl staining of brain sections showing multiple nuclei of hypothalamus: the paraventricular nucleus (PVN), lateral hypothalamic area (LHA) and anterior hypothalamic area (AHA) in (**a**), as well as dorsomedial hypothalamic nucleus (DMH), LHA, and ventromedial hypothalamic nucleus (VMH) in (**b**). The medial amygdala (MeA) is shown in (**b**) (scale bar = 1 mm).

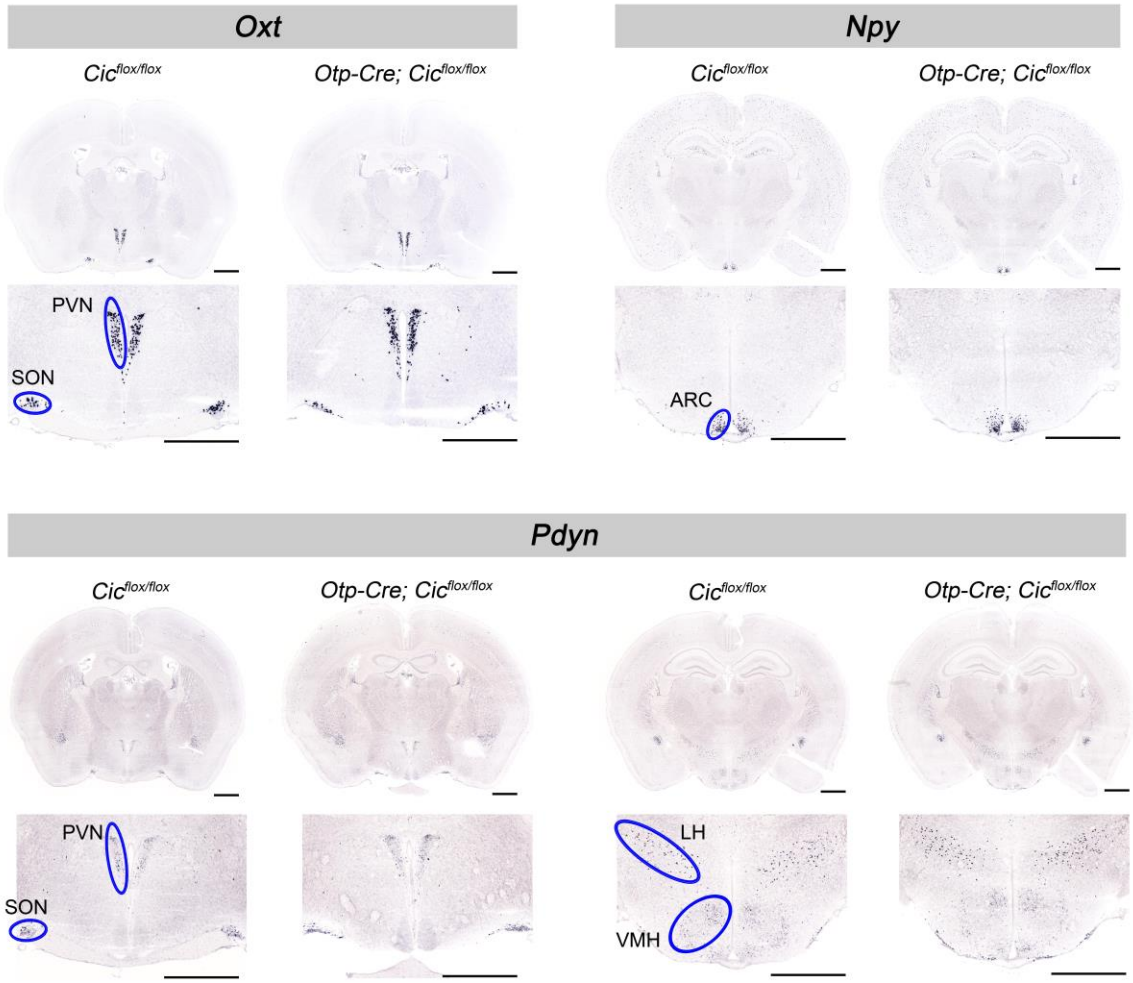

Supplementary Figure 17. Expression of neuropeptide genes is unaltered in *Otp-Cre Cic* mutant hypothalamus.

In situ RNA hybridization studies of oxytocin (*Oxt*), neuropeptide Y (*Npy*) and prodynorphin (*Pdyn*) expression showed that their expression levels and patterns were not different between control and mutant mice (scale bar = 100 μm). Whole brain images are shown in the upper panels. The regions of interest are shown in the lower panels. Representative images are shown for two to three independent experiments (n = 2-3 for each genotype). PVN, paraventricular

nucleus; SON, supraoptic nucleus; ARC, arcuate nucleus; LH, lateral hypothalamic area; VMH, ventromedial hypothalamic nucleus.

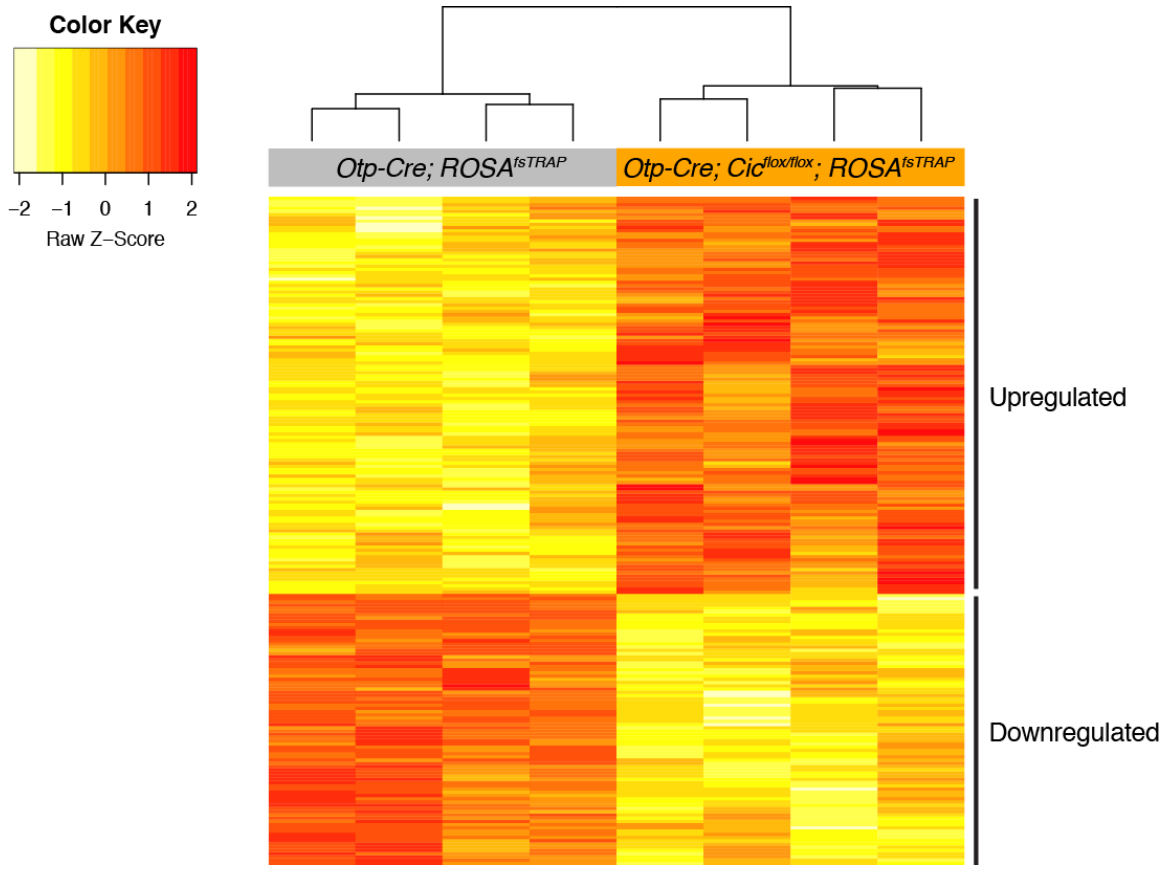

Supplementary Figure 18. Heatmap showing clustering of the differentially expressed genes from the TRAP-seq (n = 4, 8-week-old males)**.**

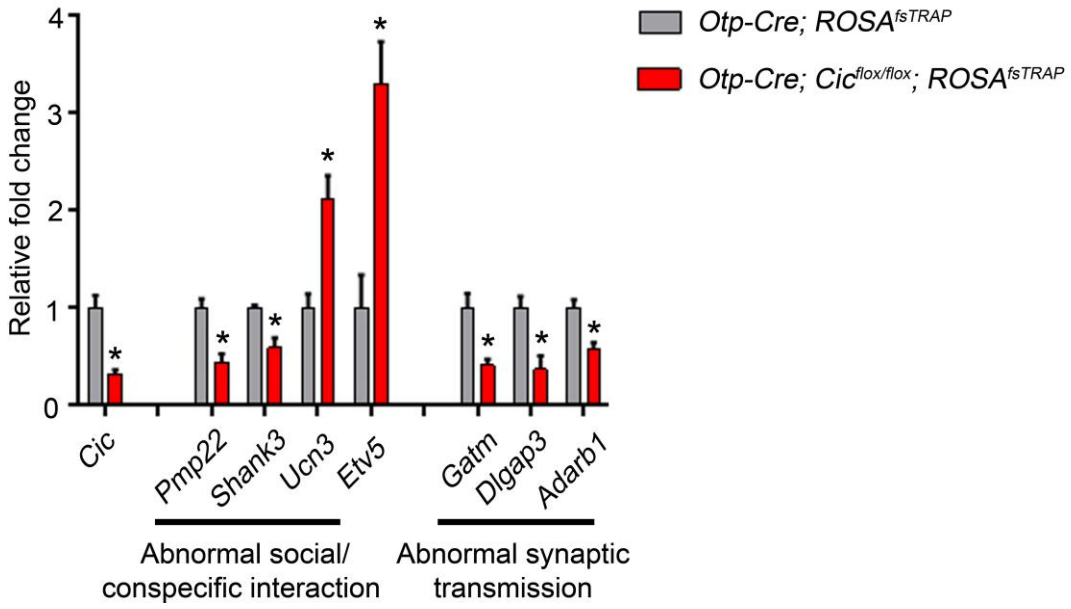

Supplementary Figure 19. TRAP-seq validation qRT-PCR.

Gene expression changes of a subset of genes were validated using quantitaitve RT-PCR. Relative fold change was caculated using house-keeping genes *Rps16*, *Hprt*, and *Gapdh*. Data are represented as mean ± s.e.m (n = 4). Statistical analysis was performed using multiple t-tests corrected for multiple comparisons using the Holm-Sidak method. *: $P < 0.05$.

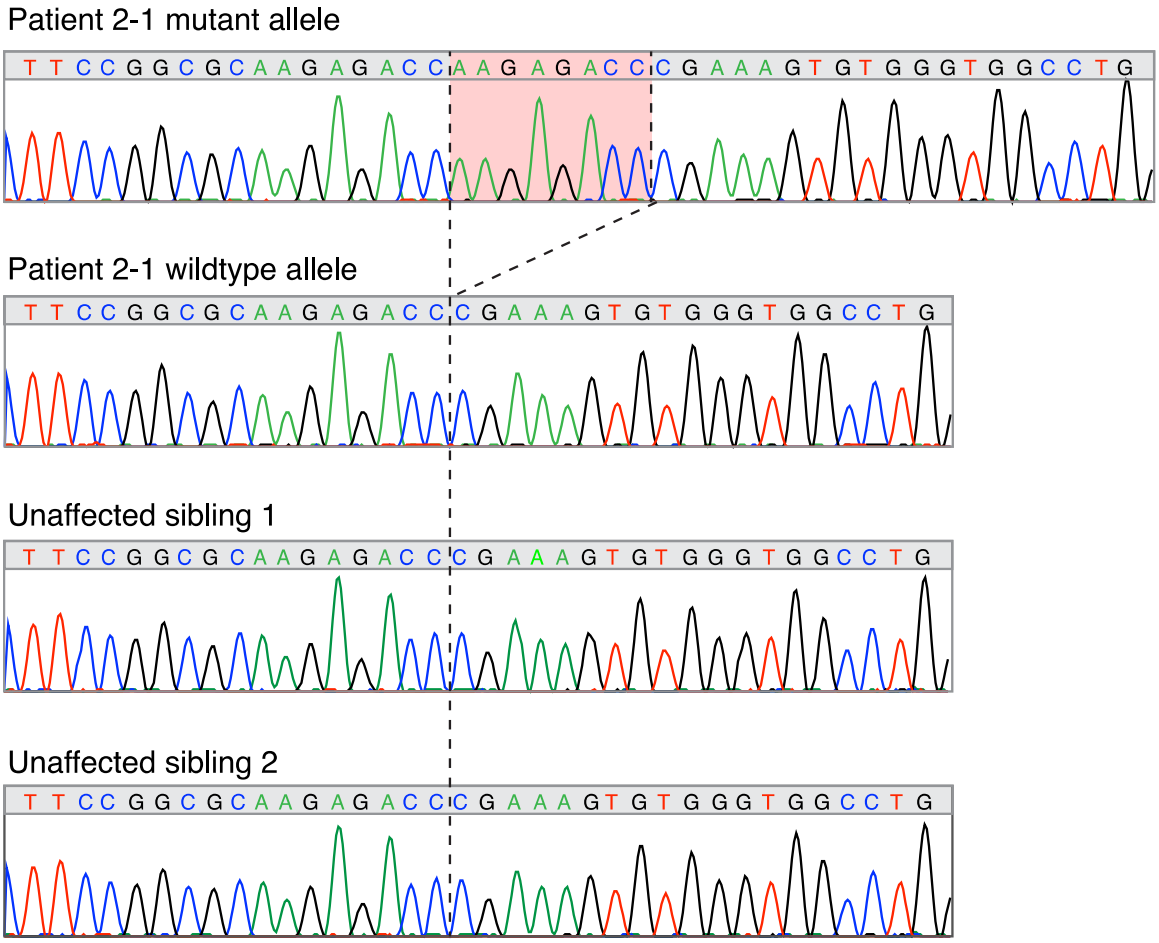

Supplementary Figure 20. Sanger sequencing results for proband's siblings in family 2. DNA from Patient 2-1 and the two unaffected sibling were amplified by PCR. For patient 2-1, the PCR products were ligated into pGEM®T-easy vectors, and individual clone was sequenced. For unaffected siblings, the PCR products were sequenced directly. The eight-nucleotide insertion (pink) can be detected in the DNA from patient 2-1, but not in the DNA from unaffected siblings.

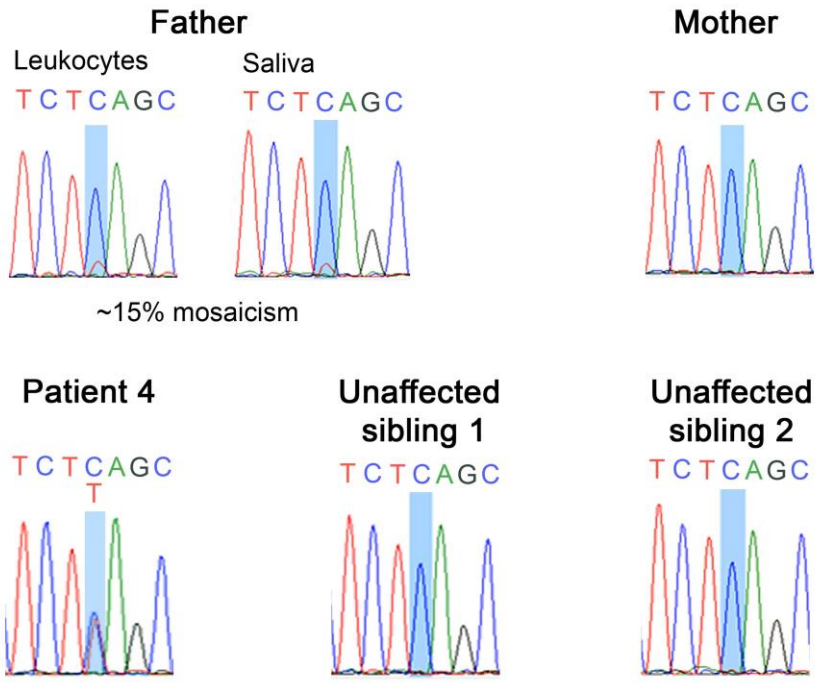

Supplementary Figure 21. Sanger sequencing results for the *CIC* variant in Family 4.

The level of mosaicism in the father was estimated from blood and saliva samples and was determined to be about 15% for the mutant allele. Patient 4 is heterozygous for the variant while the mother and the two unaffected siblings only carry the wildtype allele.

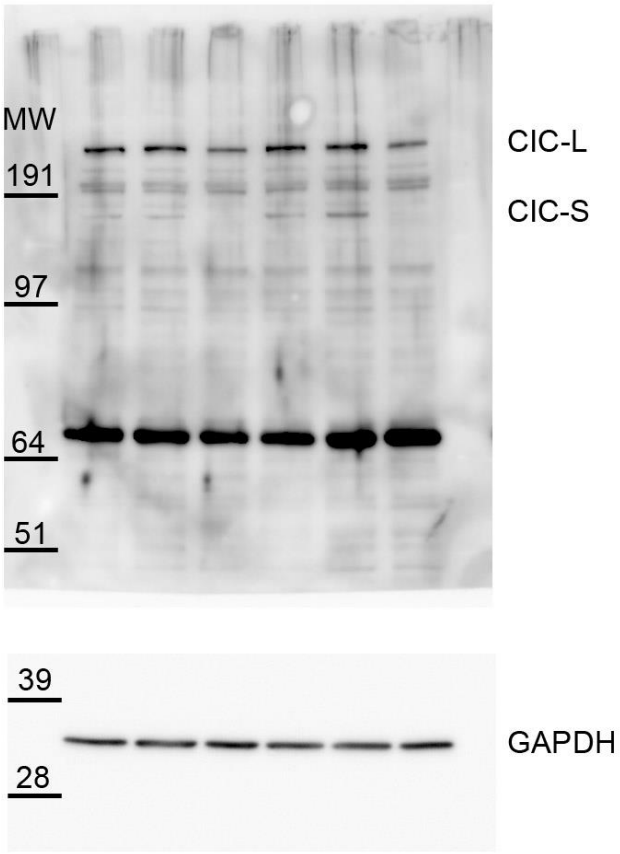

Supplementary Figure 22. Full-length western blots of Figure 6c.

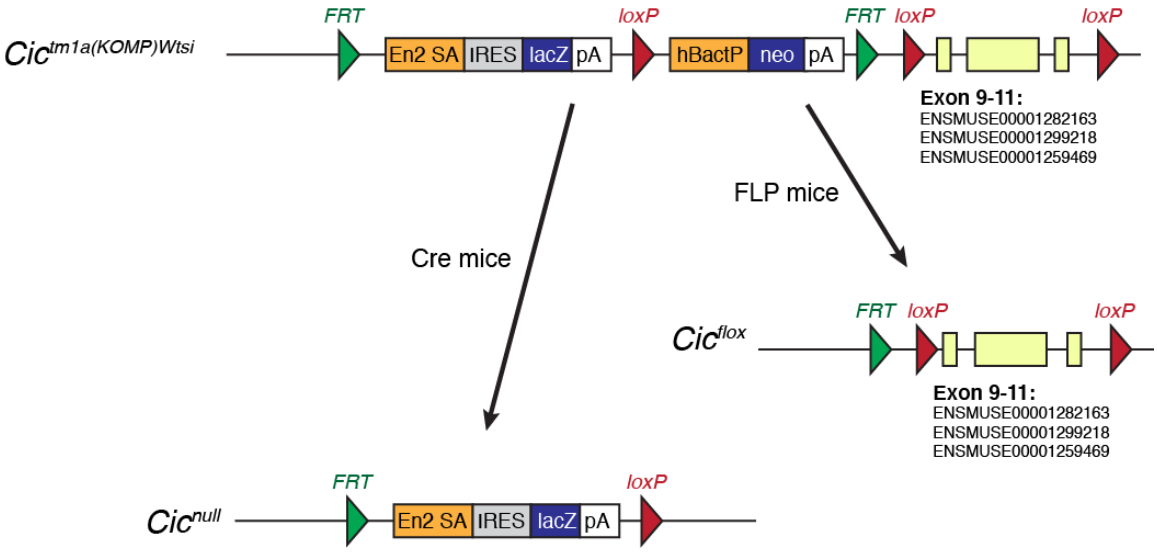

Supplementary Figure 23. Generation of *Cic*^{flox} and *Cic*^{null} alleles.

Cic^{tm1a} mice were bred to Flipper mice to remove the genetrap cassette to generate *Cic*^{flox} mice.

The *Cic*^{null} allele was generated by breeding *Cic*^{tm1a} mice to Cre deleter mice.

Supplementary Note

Patient 1

Patient 1 is a 19 year-old Caucasian female with a history of developmental delay/intellectual disability (DD/ID), autism spectrum disorder (ASD), acute lymphoblastic leukemia (ALL), cerebral folate deficiency, and epilepsy.

Pregnancy and birth history: Delivery was uncomplicated. She had neonatal hyperbilirubinemia and was found to have diastasis recti.

Summary: She was considered to have normal development until 18 months of age. At 19 months of age, she was found to have an expressive language delay due to no leap in linguistic development. At 24 months of age, there was a significant parental concern about expressive speech delay. At 26 months of age, she was diagnosed with precursor B-cell lymphoblastic leukemia (ALL) and treated with methotrexate, first with leucovorin rescue and then without. She received her final high dose of methotrexate at 32 months of age. At 39 months of age, her ALL was confirmed to be in remission status and she continued to receive treatment of low dose methotrexate till 51 months of age. At 30-36 months of age, she was noticed to have gradual developmental regression, described as loss of imaginative play skills, loss of repetitive language, and loss of motor skills. At 52 months of age, she started having choreiform movements in the right arm, as well as blinking and staring episodes. She later developed myoclonic movements of arms, complex partial seizures, and later head drops with tonic posturing. At 6 years and 7 months of age, she was found to have a mildly low level of 5-methyltetrahydrofolate in the cerebrospinal fluid (CSF) and later autoantibodies against folate receptor were detected in her CSF. At 7 years old, she had formal IQ testing and neuropsychiatry evaluation, which revealed a full scale IQ of 33 (based on Vineland Adaptive Behavior Scales, Interview Edition), and she was formally diagnosed with autism spectrum disorder.

Patient 2-1

Patient 2-1 is a 27 year-old Caucasian female with a history of seizures and pulmonic stenosis.

Pregnancy and birth history: Normal birth history with a birth weight of 7 pounds.

Summary: Parents started to notice that she had seizures when she was five years old. But parents noted that she had unexplained falls and episodes of frequent blank stares prior to developing grand mal seizures and myoclonic seizures. At 4-5 years of age, she was found to have heart murmurs, and at 9-10 years of age, she was diagnosed with pulmonic stenosis. She had an MRI at the age of five and it was normal. Her recent brain MRI was also normal. She was in special education growing up and received speech and occupational therapy. Her annual EEG has been normal and she remained seizure-free for the last ten years under anti-epilepsy medications, but her recent EMU (Epilepsy Monitoring Unit) evaluation did capture epileptiform discharges arising from right centro-parietal region.

Patient 2-2

Patient 2-2 is a 9 year-old Caucasian boy with a history of DD, seizures and ADHD.

Pregnancy and birth history: Pregnancy was complicated by intrauterine fetal growth retardation in the 3rd trimester. He was born via induced vaginal delivery at 34 weeks gestation to a 43-year-old mother. Birth weight was 5 pounds and 14 ounces.

Summary: He was diagnosed with neonatal hypoglycemia and was placed in an incubator with a nasal cannula for oxygen. Hypoglycemia resolved within 24 hours, but he remained in the neonatal intensive care unit due to difficulties in sucking during breastfeeding, and he was fed by NG-tube until he was able to suck 10 days later. At 1-2 months of age, he started having episodes of twitching movements. MRI and EEG tests were inconclusive. At around 6 months of age, he showed significant delay in both motor and language development. At 9-10 months of age, he was diagnosed with mild cerebral palsy and developmental delay, mostly gross and fine motor delay. He then started receiving early intervention therapies. He started crawling and sitting independently at around 12 months of age, and started walking at 14 months of age with the help

of ankle foot orthoses (AFOs). He began to put sentences together at 30 months of age. At 24-30 months of age, he started to have absence seizures, presented as rapid eye blinking and head twitching, several times a day. At age seven, he started to have episodes of staring spells. EEG showed frequent generalized epileptiform changes along with frequent generalized spike and wave discharges. He was diagnosed with ADHD. He has difficulties with abstract concepts and fine motor coordination. He was recently found to have a heart murmur.

Patient 3

Patient 3 is a 4 year-old Asian boy with a history of ASD, speech delay, and mild diffuse hypotonia.

Pregnancy and birth history: Pregnancy and birth were uncomplicated. He was born at full term. Birth weight was 6 pounds and 11 ounces.

Summary: Parents report that the patient developed normally until 4 months of age. He began having feeding issues, difficulties sleeping, rashes and loose stools at 3-4 months of age. These symptoms resolved on an elimination diet. Parents report that he had eye contact as a young infant and was babbling, but he lost eye contact around 6 months of age and stopped babbling at around 12 months of age. He developed self-stimulatory behaviors including flapping and spinning and perseverative behaviors. He has minimal social skills, no verbal communication, and minimal eye contact and social engagement. Brain MRI, hearing evaluation, and ophthalmologic evaluation were normal.

Patient 4

Patient 4 is a 15 year-old Caucasian boy with a history of ID, ASD, and marfanoid habitus.

Pregnancy and birth history: Pregnancy was unremarkable except for oligohydramnios. He was born full term, with a birth weight of 6 pounds and 7 ounces.

Summary: His early milestones were normal and he walked at 13 months. He had learning difficulties at school and attended a special school from 11 years of age. At 14 years old, he could only read simple sentences with little understanding, and write his name. He had behavioral issues described as autistic features (hyperactivity, stereotypic movements, and anxiety). On examination, his weight was 62 kg (+2 SD), height was 184 cm (+2.5 SD), and head circumference was 54 cm (+1 SD). He had a marfanoid habitus: scoliosis, arachnodactyly, flat feet, slender built. He had an electroencephalogram when he was five years old, that showed an aspecific abnormal pattern. He now has inappropriate laughing episodes, and a control EEG will be planned. His brain MRI showed non-specific white matter signal anomalies.